Propagation of Degenerate Band-Edge Modes Using Dual Nonidentical Coupled Transmission Lines

A. Muhammed Zuboraj,* B. Kubilay Sertel,† and C. John L. Volakis‡

ElectroScience Laboratory, Department of Electrical and Computer Engineering, The Ohio State University, Columbus, Ohio 43212, USA

(Received 26 November 2016; revised manuscript received 15 March 2017; published 28 June 2017)

Degenerate band-edge (DBE) modes are known for their exceptionally high field intensity at the nearly flat dispersion-diagram profile. Because of the latter property, resonances supported by these modes are associated with a very strong field at the band edge. DBE modes and similar resonances of this class have been typically realized by introducing anisotropic dielectric slabs in volumetric photonic crystals. By contrast, in this paper, we present an analytic model of DBE modes using a simple set of nonidentical coupled transmission lines. The unequal phase velocities of the supported waves supported by these transmission lines lead to mode degeneracy, that in turn provide quartic solutions of dispersion (ω-β) relations. The DBE mode appears as one these quartic solutions. As such, the proposed model generalizes the concept of DBE modes using the construct of nonidentical coupled transmission lines. In this paper, we also propose a propagation medium using a dual pair of nonidentical transmission lines. The medium is referred to as a "butterfly" structure and is composed of four coupled transmission lines. These four coupled transmission lines generate the TM_{01}-like degenerate band-edge mode. This is done by coupling the TE modes supported on each pair of the transmission lines. Mode purity at the resonance frequency and the intense field profile on the axis are properties that can be exploited for high-power microwave sources.

DOI: 10.1103/PhysRevApplied.7.064030

I. INTRODUCTION

Periodic and/or metamaterial structures are routinely used to control propagation characteristics of electromagnetic waves. They have been successfully used in numerous applications, including antenna arrays [1], leaky-wave antennas [2], electromagnetic band-gap structures [3], artificial magnetic conductors [4], frequency selective surfaces [5], and slow-wave realization [6–8]. Depending on the unit elements used in periodic layers, different properties of electromagnetic-wave propagation are achieved. For example, (i) using split rings and copper strips in a two-dimensional periodic array, a negative index of refraction is achieved [9]; (ii) periodically spaced antenna elements provide arbitrary beam forming for multipath signal reception and target tracking [10,11]; (iii) a two-dimensional textured lattice of resonant elements in a metal sheet forms a high impedance surface, preventing certain frequencies from propagation [4]. However, the simplest form of periodic structures is periodic dielectric stacks that have been traditionally used to achieve electromagnetic band gaps [12]. In this paper, we focus on the latter and propose a replacement of those dielectrics using coupled transmission lines.

Periodic stacks of dielectrics are often referred to as photonic crystals, as in Fig. 1(a). These crystals support band gaps in their dispersion diagrams caused by the coupling of forward and backward waves. The actual dispersion curve can be of the second order with the edge of the band gap located at the $\beta p = \pi$ point, referred to as the "regular band edge" (RBE) [Fig. 1(a)]. Field intensity is typically high at the band edge and is proportional to N^2 [13], where N is the number of periodic cells in an array.

When anisotropic dielectric layers are used to form unit cells of the stack, additional resonances can be supported [7,14,15]. The dispersion diagram for these cases can be up to the fourth order and the edge of the band is usually referred to as the degenerate band edge (DBE) [15,16]. Because of this fourth-order ω-β relation, the field intensity at the band edge is proportional to N^4 [13,15], where N is the number of periodic cells in an array. That is, a huge field enhancement is associated with this resonance realized by these special DBE crystals [13,15]. This property has been exploited in the past to improve the directivity of dipole antennas [17]. The insertion of a magnetic layer into the unit cell can generate magnetic photonic crystal modes [8,18]. These modes are especially useful to achieve frequency-independent scanning of leaky-wave antennas [2].

Despite their attractive properties and applications, DBE crystals lack simplicity in realization. These crystals are usually formed of bulk dielectric slabs and require large space. Because of this, the DBE crystals are difficult to

*zuboraj.1@buckeyemail.osu.edu
†sertel.1@osu.edu
‡volakis.1@osu.edu

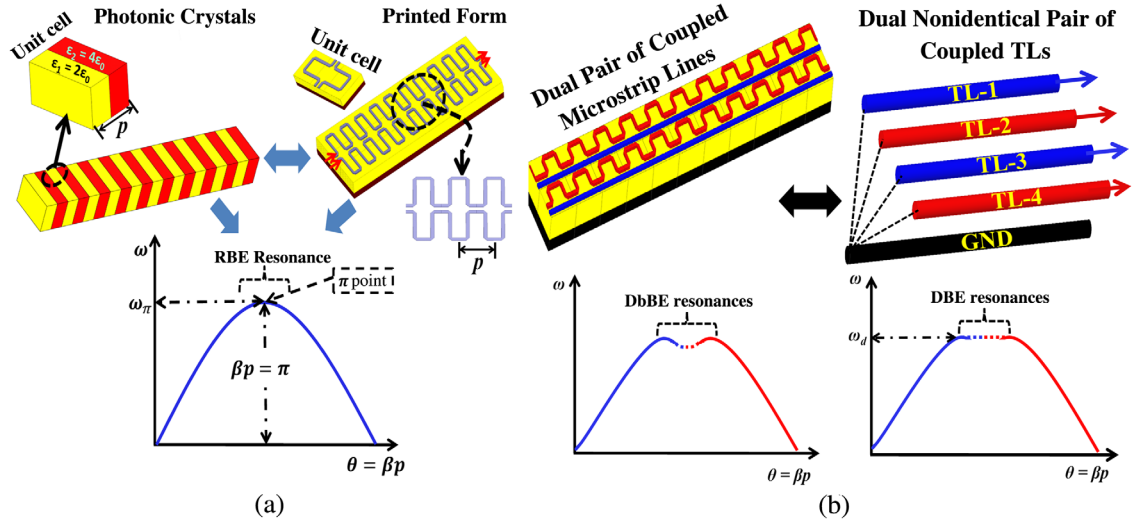

FIG. 1. (a) 1D photonic crystals composed of dielectric stacks (top left); equivalent medium in the form of printed circuits (top right); ω-β diagram showing regular band-edge resonance (bottom). (b) Dual pair of coupled nonidentical microstrip lines and its equivalent circuit; DbBE (bottom left) and DBE (bottom right) resonances are supported on these lines.

conform into certain applications, e.g., electronic chips, planner antennas, waveguides, etc., where space is limited. Therefore, alternate approaches to realizing such media are of interest. As shown in Refs. [13,19,20], the physics of DBE and MPC modes are associated with anisotropic media and a special mode-coupling mechanism. Already, as a simpler alternative, Locker *et al.* [7] introduced the concept of coupled transmission lines (TLs) to emulate photonic crystals. As shown by Locker *et al.* [7], coupled and uncoupled sections of meandered microstrip lines emulate the required anisotropy for the realization of DBE modes. This approach has also been used to realize miniaturized antennas [6] and to achieve frequency-independent beam scanning [2] in leaky-wave antennas.

Although the concept of coupled TLs has been successfully used [21] in various applications, its potential has yet to be exploited. For example, DBE modes have yet to be realized inside waveguide structures. Recently, Othman *et al.* [22] proposed a medium formed by misaligned elliptic irises that demonstrates DBE modes inside circular waveguides. These modes can be useful to amplify the rf wave that interacts with an electron beam [23] in traveling-wave tubes and/or backward-wave oscillators (BWOs). Typically, the electronic efficiency of traveling-wave tubes and BWOs is low and dependent on the axial field intensity of the waveguide modes. Therefore, the introduction of alternative modes within the waveguide that support a strong axial electric field at the center can improve beam-to-rf mode interactions. However, the elliptic irises [22] do not support pure TM_{01} modes, an essential property for efficient beam-wave interactions. Even though the DBE mode is demonstrated in dispersion diagrams [22], the physics of mode coupling in the presence of the natural TE and TM modes inside has not been explained. To do so, a generalized approach of the mode-coupling mechanism is introduced in this paper.

We present a generalized method of mode coupling using nonidentical coupled transmission lines to realize fourth-order dispersion diagrams (DBE modes). In previous papers [7,8], only a single pair of coupled TLs was considered and the associated coupled modes were TEM types. However, a single pair of nonidentical TLs does not provide sufficient coupling to support DBE modes due to the presence of the natural waveguide (TE, TM) modes in the background. Also, in previous works, the coupling was not characterized in terms of simple (L, C) parameters. Further, as noted above, the mode-coupling mechanisms leading to higher-order dispersion were not explained.

In this paper, we build upon the concept of coupled transmission lines and proceed to generate higher-order dispersion curves using a "coupled-mode" technique for dual pairs of nonidentical coupled TLs [Fig. 1(b)]. The key characteristics of the coupled TLs are the following: (i) nonidentical TLs; (ii) coupled (L, C) parameters; and (iii) coupling coefficients, later defined as K_{c1}, K_{c2}, and K_{c3}. These will be explained in Sec. II. Section III presents a "butterfly" structure that realizes the nonidentical TLs. The structure demonstrates DBE modes with a TM_{01}-like field profile. In Sec. IV, a BWO example will be given as a sample of vacuum-tube applications using four coupled transmission lines. It is shown that the field enhancement due to the DBE mode improves the BWO's electronic efficiency. Overall, we believe that the findings and analysis in this paper will provide a basis for dispersion engineering pertaining to other applications such as resonator antennas [24], waveguides [25], and cavities [26].

II. DISPERSION ENGINEERING USING DUAL NONIDENTICAL PAIR OF TLs

A. Background

Transmission lines are inherently periodic structures, as they can be modeled with periodically spaced lumped elements (L, C) of period p. TLs support both forward and backward waves. By controlling the (L, C) parameters of the TLs, slow waves ($v \ll c$) can be realized. Indeed, this property has been used to enhance the coupling of the electron beam to rf waves in traveling-wave tubes and BWO applications. Examples of coupled transmission lines include double helix [27], ring bar [28,29], and ring loop [30], etc. For these cases, the TL pair has identical lumped elements (L, C) and supports the regular band-edge mode only. This mode is observed at the frequency (ω_π) corresponding to $\beta p = \pi, 3\pi, 5\pi, \ldots$. in the dispersion diagram, where β is the propagation constant and ω_π is the angular frequency. We remark that regular band-edge resonances are a consequence of the coupling between the forward and backward-wave modes [29,31,32].

When the coupled TLs are not identical, viz., composed of different lumped elements (blue and red) as shown in Fig. 1(b) (top), the forward and backward waves have unequal phase and group velocities and give rise to the double band edge (DbBE) as in Fig. 1(b) (bottom left). The term "double band" originates from the presence of dual RBE resonances in the dispersion diagram. Typically, DbBE resonances are weak in comparison to DBE resonances and are not useful since the field intensity at the band edge is proportional to N^2. The nonidentical nature of the TLs induces weak coupling between two RBE resonances, creating a crest in between them [Fig. 1(b)]. The latter affects the electric field intensity at the band edge. The coupling strength between these two RBE resonances is completely dependent on the type of mode involved, i.e., the field profiles of each mode.

In contrast, DBE modes are quite strong due to their degeneracy at the band edge. The coupling strength between the TLs, if chosen appropriately by modifying the geometry of rf structure, furnishes an appropriate coupling environment required for DbBE modes to evolve into DBE modes [Fig. 1(b), bottom right]. Therefore, DBE resonance can be achieved if the lumped parameters of the nonidentical coupled TLs are chosen appropriately. Unlike DbBE resonances, four modes are strongly coupled together to form DBE resonances. Because of this, field intensity at the band edge is a couple of degrees higher as compared to RBE or DbBE resonances. Actually, more than second-order dispersion can be achieved using a pair of nonidentical coupled TLs. Depending on the modes involved in the coupling process and lumped (L, C) elements, DbBE or DBE modes can be achieved. Below, we provide a theoretical analysis for the coupled TLs to generate higher-order dispersion curves.

B. Theoretical analysis

The presented analysis follows the coupled-mode theory [31,33]. For any continuously coupled system, the coupled-mode propagation constants are functions of the propagation constants of each uncoupled mode [31]. For detailed information about the continuous coupling in periodic systems and the associated propagation constants, please refer to the derivation in the Supplemental Material [34]. Since coupled TLs comprise periodically spaced lumped coupling elements (L_M, C_M), the analogy of the continuously coupled system can be translated to the coupled transmission-line systems. Accordingly, the coupled pair of TLs are associated with the propagation constants [31]:

$$\beta_\pm = \frac{\beta_m + \beta_n}{2} \pm \sqrt{\left(\frac{\beta_m - \beta_n}{2}\right)^2 - K_c^2}. \tag{1}$$

Here, $\beta_m = \omega\sqrt{LC}$, $\beta_n = (2\pi/p) - \omega\sqrt{LC}$, the uncoupled propagation constants of each line being coupled and $\beta_\pm$ refer to the forward and backward modes for the coupled TL system. Also, the coefficient K_c represents the coupling between the β_{mn} modes. We remark that Eq. (1) is the building block of our analysis. Specifically, by choosing appropriate modes to replace the (β_m, β_n) pair, fourth-order dispersion curves can be generated.

To begin, let us consider two uncoupled TLs associated with different lumped inductances and capacitances (L_1, C_1) and (L_2, C_2). These lines are depicted in blue and red in Figs. 2(a) and 2(b). Each TL supports forward and backward waves associated with unequal velocities $v_1 = (1/\sqrt{L_1C_1}) \neq (1/\sqrt{L_2C_2}) = v_2$. The propagating constants of these four waves are

$$\beta_a = \omega\sqrt{L_1C_1} = \frac{\omega}{v_1}, \tag{2}$$

$$\beta_b = \frac{2\pi}{p} - \omega\sqrt{L_1C_1} = \frac{2\pi}{p} - \frac{\omega}{v_1}, \tag{3}$$

$$\beta_c = \omega\sqrt{L_2C_2} = \frac{\omega}{v_2}, \tag{4}$$

$$\beta_d = \frac{2\pi}{p} - \omega\sqrt{L_2C_2} = \frac{2\pi}{p} - \frac{\omega}{v_2}. \tag{5}$$

Each of the above β's gives rise to the linear dispersion curves (2)–(5) in Fig. 2(c). Notably, unlike identical TLs, each line supports nonoverlapping forward-wave and backward-wave modes represented by solid and dashed lines, respectively. We denote the forward-wave propagation constants as β_a (solid blue line) and β_c (solid red line). Similarly, β_b (dashed blue line) and β_d (dashed red line) represent the backward-wave propagation constants.

When the TLs are coupled, they couple through the forward and backward mode pairs. This gives rise to

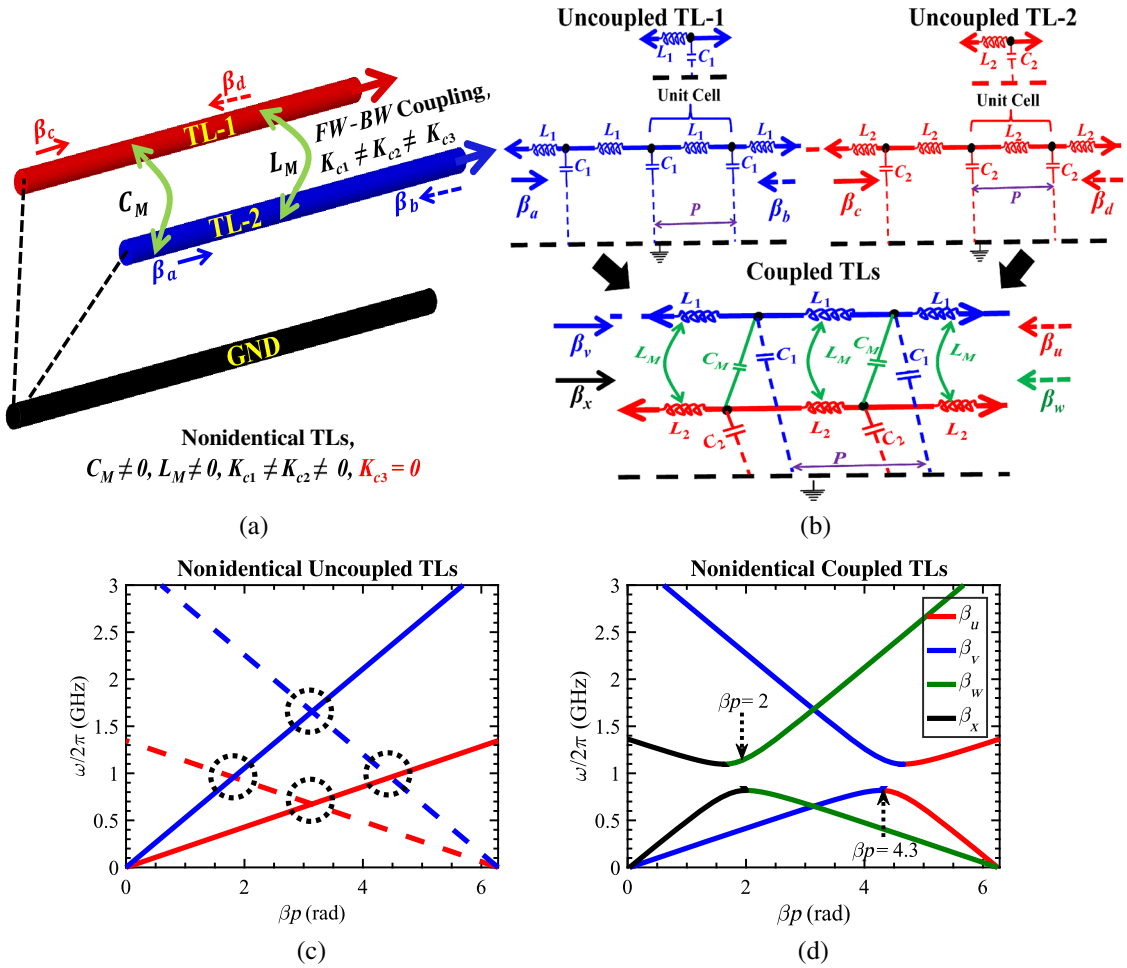

FIG. 2. (a) A pair of coupled nonidentical TLs to realize DbBE and DBE modes. Two oppositely traveling waves with unequal phase velocities couple through mutual inductance L_M and capacitance C_M. (b) Pair of uncoupled and coupled nonidentical TLs supporting forward and backward waves whose propagation constants are defined in Eqs. (2)–(9). (c) ω-β dispersion diagram of the uncoupled TLs for each of the supported modes given in Eqs. (2)–(5). The solid blue line and solid red line represent Eqs. (2) and (4), while the dashed blue line and dashed red line represent Eqs. (3) and (5). (d) Regular band-edge resonances realized by the nonidentical coupled TLs are found due to unequal velocities (v_1, v_2), Eqs. (6)–(9). These curves refer to circuit parameters $(L_1, C_1) \equiv (16.17\ \mu\text{H}, 68.8\ \text{pF})$ and $(L_2, C_2) \equiv (6.5\ \mu\text{H}, 27.52\ \text{pF})$.

second-order dispersion curves as in Fig. 2(d). Specifically, the coupling between forward and backward mode pairs, e.g., $\beta_a(\omega)$, $\beta_d(\omega)$ and $\beta_b(\omega)$, $\beta_c(\omega)$ gives rise to second-order dispersion curves. The associated propagation constants are given by

$$\beta_u = \frac{\pi}{p} - \frac{\omega}{2}\left(\frac{1}{v_2} - \frac{1}{v_1}\right) + \sqrt{\left\{\frac{\pi}{p} - \frac{\omega}{2}\left(\frac{1}{v_2} + \frac{1}{v_1}\right)\right\}^2 - K_{c1}^2}, \tag{6}$$

$$\beta_v = \frac{\pi}{p} - \frac{\omega}{2}\left(\frac{1}{v_2} - \frac{1}{v_1}\right) - \sqrt{\left\{\frac{\pi}{p} - \frac{\omega}{2}\left(\frac{1}{v_2} + \frac{1}{v_1}\right)\right\}^2 - K_{c1}^2}, \tag{7}$$

$$\beta_w = \frac{\pi}{p} + \frac{\omega}{2}\left(\frac{1}{v_2} - \frac{1}{v_1}\right) + \sqrt{\left\{\frac{\pi}{p} - \frac{\omega}{2}\left(\frac{1}{v_2} + \frac{1}{v_1}\right)\right\}^2 - K_{c2}^2}, \tag{8}$$

$$\beta_x = \frac{\pi}{p} + \frac{\omega}{2}\left(\frac{1}{v_2} - \frac{1}{v_1}\right) + \sqrt{\left\{\frac{\pi}{p} - \frac{\omega}{2}\left(\frac{1}{v_2} + \frac{1}{v_1}\right)\right\}^2 - K_{c2}^2}. \tag{9}$$

It is noted that Eqs. (6)–(9) represent second-order dispersion curves and are associated with regular band-edge resonances at $\beta p = 2$ (rad) and $\beta p = 4.3$ (rad), respectively. Their associated dispersion curves are given in Fig. 2(d).

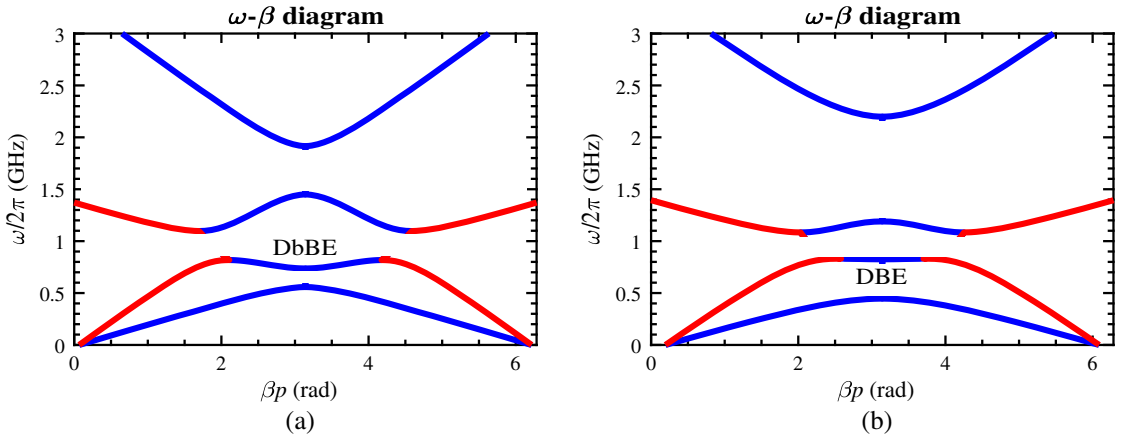

FIG. 3. ω-β diagrams associated with coupled pairs of TLs. The (L, C) parameters of the coupled TLs of each pair are $(L_1, C_1) \equiv (16.17\ \mu\text{H}, 68.8\ \text{pF})$ and $(L_2, C_2) \equiv (6.5\ \mu\text{H}, 27.52\ \text{pF})$. (a) DbBE dispersion curves, viz., weak coupling of the dual TL pair. For the DbBE mode, the coupling parameters are $K_{c1} = K_{c2} = K_{c3} = 20.85$. (b) DBE dispersion curves, viz., strong coupling of the dual TL pair. These are fourth-order curves and higher-order dispersion condition: $(\partial^3\omega/\partial\beta^3) \neq 0$, the coupling parameters are $K_{c1} = K_{c2} = 20.85 \neq 50 = K_{c3}$.

To characterize and observe higher-order coupling, we introduce a coupling parameter K_{c3}. This quantity represents coupling between β_v and β_w. Since β_v and β_w have the same phase velocity at the π point, these pairs couple further inside the waveguide and form fourth-order dispersion curves.

$$\beta_1 = \frac{\pi}{p} + \sqrt{\left[\frac{\omega}{2}\left(\frac{1}{v_1} - \frac{1}{v_2}\right) - \sqrt{\left\{\frac{\pi}{p} - \frac{\omega}{2}\left(\frac{1}{v_1} + \frac{1}{v_2}\right)\right\}^2 - K_{c1}^2}\right] - K_{c3}^2}, \tag{10}$$

$$\beta_2 = \frac{\pi}{p} - \sqrt{\left[\frac{\omega}{2}\left(\frac{1}{v_1} - \frac{1}{v_2}\right) - \sqrt{\left\{\frac{\pi}{p} - \frac{\omega}{2}\left(\frac{1}{v_1} + \frac{1}{v_2}\right)\right\}^2 - K_{c1}^2}\right] - K_{c3}^2}, \tag{11}$$

$$\beta_3 = \frac{\pi}{p} + \sqrt{\left[\frac{\omega}{2}\left(\frac{1}{v_1} - \frac{1}{v_2}\right) - \sqrt{\left\{\frac{\pi}{p} - \frac{\omega}{2}\left(\frac{1}{v_1} + \frac{1}{v_2}\right)\right\}^2 - K_{c2}^2}\right] - K_{c3}^2}, \tag{12}$$

$$\beta_4 = \frac{\pi}{p} - \sqrt{\left[\frac{\omega}{2}\left(\frac{1}{v_1} - \frac{1}{v_2}\right) - \sqrt{\left\{\frac{\pi}{p} - \frac{\omega}{2}\left(\frac{1}{v_1} + \frac{1}{v_2}\right)\right\}^2 - K_2^2}\right] - K_{c3}^2}. \tag{13}$$

The corresponding propagation constants β_2 and β_3 are of fourth order and can be derived using the process described in Ref. [31].

When Eqs. (10)–(13) are plotted in Fig. 3, DbBE and DBE modes are observed subject to appropriate choices for K_{c1}, K_{c2}, and K_{c3}. That is, K_{c3} is important in realizing higher-order dispersion curves.

Above, K_{c1}, K_{c2}, and K_{c3} signify different mode-formation mechanisms. It is noted that these parameters are strongly dependent on geometric features and mode profile. For example, the parameters K_{c1} and K_{c2} represent natural coupling between the forward and backward modes of two nonidentical TLs. Each of the forward-wave and backward-wave velocities can be nonidentical to each other and the degree of coupling is strongly dependent on their field profile.

On the contrary, K_{c3} represents the coupling between two RBE resonances of two different modes. Therefore, the derivation of K_{c3} is a cumbersome process and is beyond the scope of this paper. Indeed, a numerical approach can be employed to compute K_{c3}.

We note that special choices for K_{c1}, K_{c2}, and K_{c3} lead to the realization of DbBE [Fig. 3(a)] and DBE modes [Fig. 3(b)]. For example, a strong flattop fourth-order

resonance (DBE mode) is observed for $K_{c1} = K_{c2} \neq K_{c3}$ [Fig. 3(b)]. Since the ω-β diagram is a fourth-order polynomial, i.e., $\omega \propto (\beta^4)$, the first, second, and third derivatives of ω are nonzero at the band edge. This is an important property that verifies the presence of the DBE modes in the dispersion diagram. Recently, Othaman *et al.* [23] demonstrated that DBE modes can be realized by imposing angular anisotropy using elliptic irises in the circular waveguide. In the following section, we present an example of such DBE mode realization using coupled TLs.

III. REALIZATION OF THE DBE MODE USING BUTTERFLY GEOMETRY

Above, we proposed a pair of nonidentical TLs to realize higher-order dispersion curves. However, depending on the geometry and mode profile, the coupling parameters are affected and either the DbBE or DBE mode is observed. In this section, we present an example of rf structure based on coupled TLs placed inside a waveguide. As already stated, strong coupling among the nonidentical coupled TLs is necessary to achieve DBE modes. Othman *et al.* [22] demonstrated such a medium by using misaligned elliptic irises placed on the axis of a circular waveguide.

In this paper, we realize DBE modes using two pairs of freestanding wire TLs placed orthogonally to each other. One such structure is demonstrated in Fig. 4(a). The associated structure is formed by a butterfly unit cell. This unit cell is composed of two nonidentical pairs of TLs represented by elliptic wires and bars, marked as blue and red in Fig. 4(b). Notably, the four TLs are placed circularly among a set of rings. These rings serve to realize coupling among the four TLs. Each pair of TLs (blue or red) are in essence curved ring-bars [29]. The coefficients, K_{c1} and K_{c2} represent the coupling between oppositely traveling modes for the TL pairs. They are given as follows [29]:

$$K_{c1} = \frac{(1+\frac{\pi h_a}{4a})}{E_1(m)}\sqrt{\frac{\beta_a\beta_d}{|\beta_a-\beta_d|}}, \tag{14a}$$

$$K_{c2} = \frac{(1+\frac{\pi h_b}{4a})}{E_2(m)}\sqrt{\frac{\beta_b\beta_c}{|\beta_b-\beta_c|}}, \tag{14b}$$

where $E_1[m=(h_a/h_c)] = \int_0^{\pi/2}\sqrt{1-(m^2-1)\sin^2(\theta)}d\theta$ and $E_2[m=(h_b/h_c)] = \int_0^{\pi/2}\sqrt{1-(m^2-1)\sin^2(\theta)}d\theta$ is the elliptic integral of the second kind.

In Fig. 4(a), the coupling rings are marked with a green color and allow control of mutual inductances and capacitances between the TL pairs. It is noted that each identical pair (blue or red) in Fig. 4 serves as a single TL component of the nonidentical TL model as shown in Fig. 2(b). This coupling mechanism serves to

(i) Provide a medium that support slow waves.
(ii) Lower the cutoff frequency of waveguide modes.
(iii) Facilitate coupling of the lower-order modes to form a higher-order mode such as the DBE mode.

To illustrate the above mechanism, we refer to Figs. 5(a) and 5(b). Indeed, the introduction of butterfly geometry lowered the cutoff frequency of each mode forming slow waves inside the circular waveguide as shown in Fig. 5(b). As depicted in Fig. 5(c), the degenerate TE_{11} mode coupled to the TE_{21} mode to form the DBE TM_{01}-like resonance.

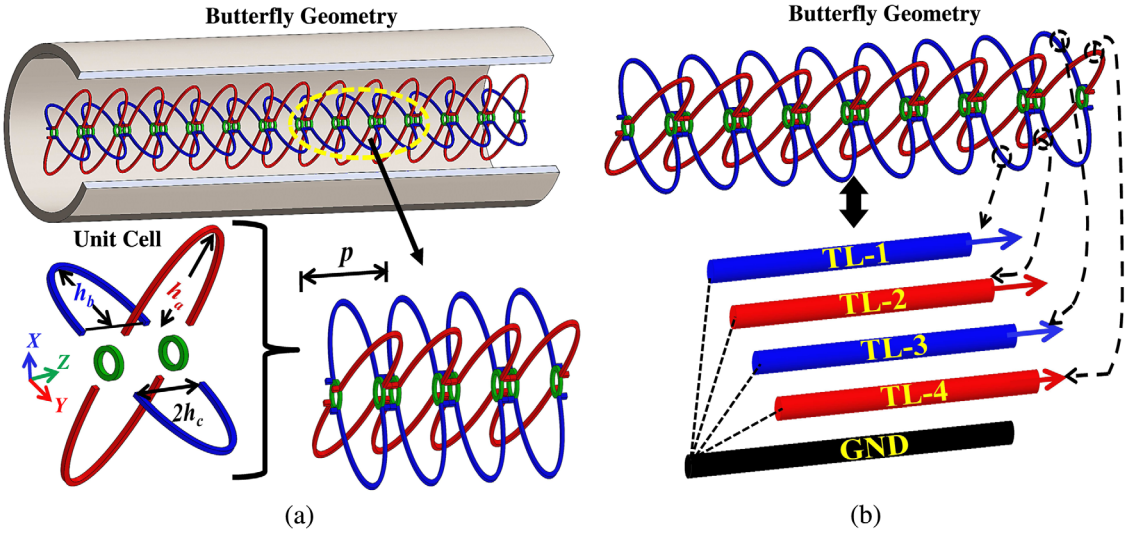

FIG. 4. (a) The butterfly slow-wave structure placed within a circular waveguide for realizing DBE modes. The unit cell is shown below the circular waveguide. Each of the four TLs is formed of a series of elliptical loops. Also, a ring at the center of the TLs serves to achieve coupling among the TLs. The dimensions of the elliptical and circular rings are $h_a = 50.8$ mm, $h_b = 36.4$ mm, $h_c = 7.4$ mm, $p = 22$ mm, $r_b =$ ring radius $= 4.5$ mm, $r_g =$ waveguide radius $= 63.5$ mm. Notably, the unequal pairs in different planes emulate nonidentical coupled TLs. (b) Butterfly geometry and its equivalent TL structure.

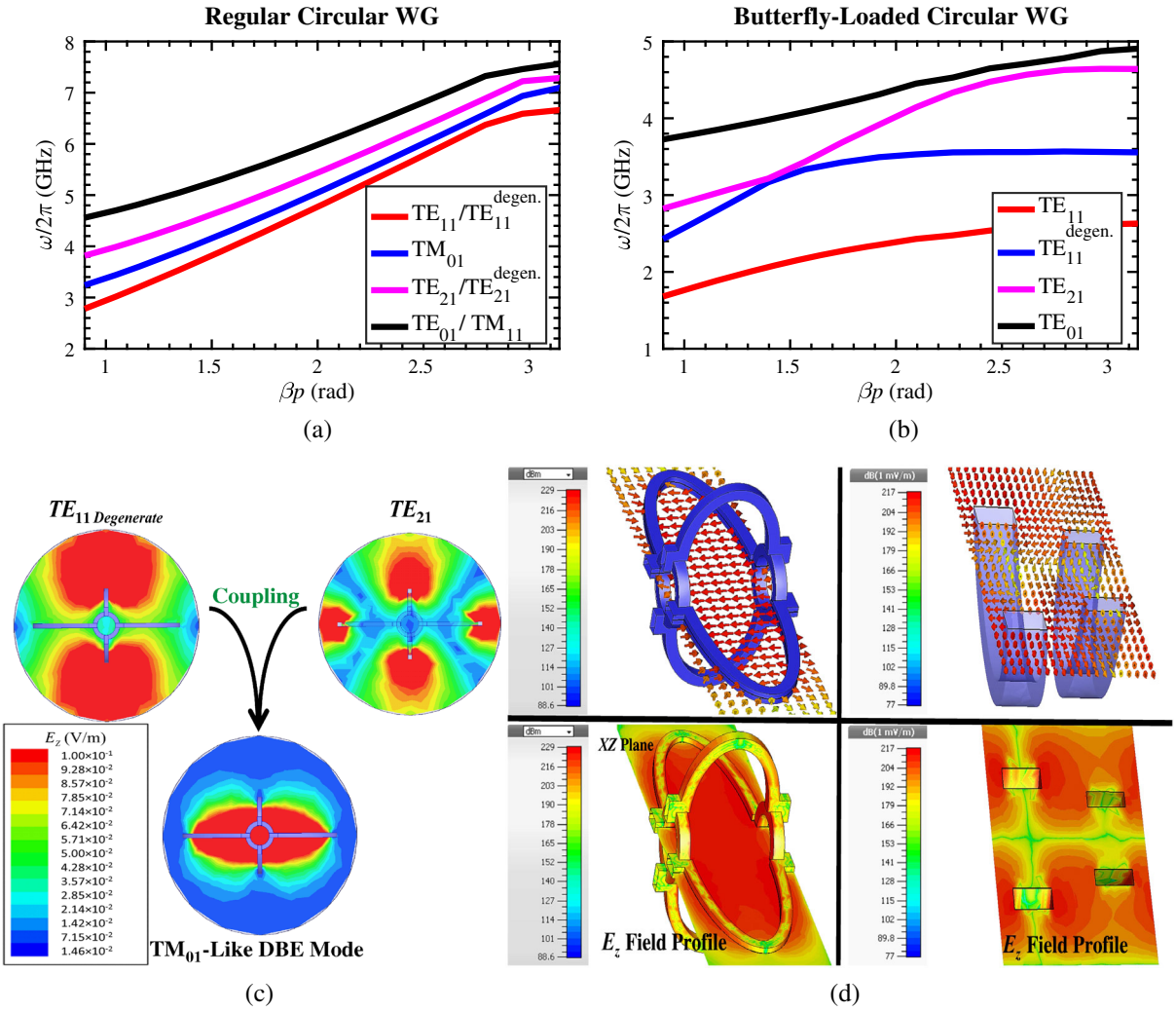

FIG. 5. Comparison of the dispersion diagrams with (a) and without (b) the butterfly periodic geometry inside the circular waveguide. As seen, the introduction of the butterfly TL structure lowers the cutoff frequency of each mode by splitting the TE_{11} degenerate modes. (c) Illustration of coupling to form the DBE TM_{01} mode by coupling of TE_{21} and TE_{11} degenerate modes is shown. The field profiles are magnitudes of the overall field amplitude with E normalized to 0.1 V/m. (d) (top) Overall electric field magnitude, E and E_z field magnitude (bottom) in the XY plane at the DBE resonance of the butterfly geometry and elliptical iris-loaded waveguide [22]. The units are in decibels (1 mV/m) [35].

We remark that coupling is achieved via the mutual H_z fields supported by the TE_{11} and TE_{21} modes. It is noted that unlike DBE crystals, no band gap is observed in dispersion diagrams. This is due to the presence of other higher-order waveguide modes in the waveguide which are not affected by the geometry. One key property of the butterfly geometry is its strong E_z field that leads to a strong TM_{01}-like mode at the DBE resonance. As shown in Fig. 5(d), the strong and uniform E_z provides mode purity as compared to the elliptic iris-loaded waveguide [22]. In fact, the E_z field at the center ($r = 0$), is approximately 300 times stronger than that of the elliptical iris-loaded waveguide as shown in Fig. 6(a). Therefore, the purity of the mode supported by the strong DBE resonance is suitable for vacuum-tube devices where the strong E_z field is required. The provided field profiles are obtained from CST Microwave Studio [35]. The detailed dispersion diagram for the DBE mode of butterfly structure is obtained via full-wave simulation using the Ansoft High Frequency Simulation Software (HFSS) package, 2015 [36]. It is also verified using the Computer Simulation Technology (CST) Microwave Studio [35]. It is shown in Fig. 6(b). The resonant frequency of the DBE TM_{01}-like mode is observed at approximately $\omega_d = 3.52$ GHz.

The above geometry utilizes the property of curved ring-bar unit cells, known for supporting the TM_{01} mode. For the other geometry, the mode profile defines the (L, C) parameters. The challenge is to model each mode to its

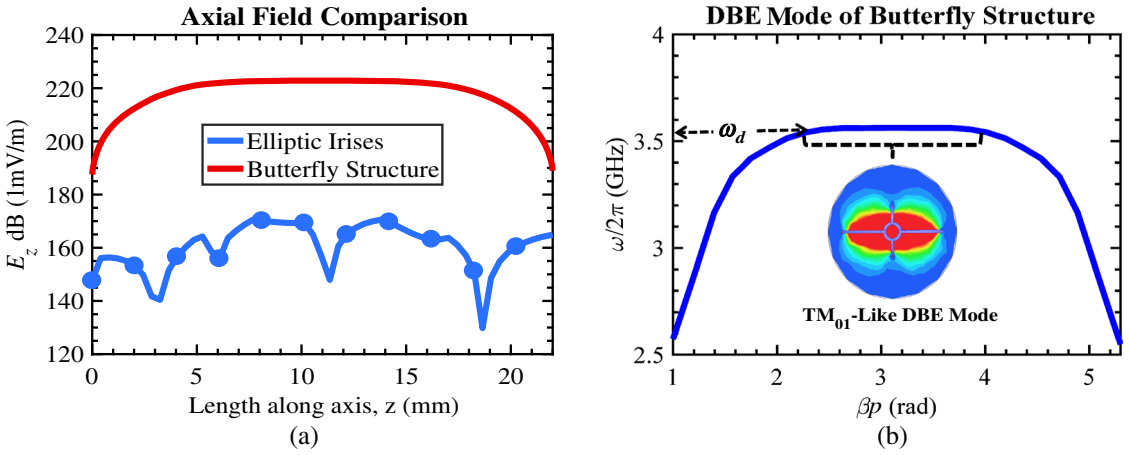

FIG. 6. (a) A comparison of the E_z field along the axis of butterfly geometry and the elliptical iris-loaded waveguide. As shown, butterfly geometry provides E_z approximately 300 times larger compared to elliptic irises [22]. (b) ω-β diagram of the butterfly structure. The DBE mode is depicted along with its field profile. The DBE resonance is observed at $\omega_d/2\pi = 3.52$ GHz.

transmission-line equivalents and find the appropriate coupling parameters: K_{c1}, K_{c2}, and K_{c3}. Hence, the above approach forms a mathematical tool for all.

IV. BWO DESIGN USING BUTTERFLY STRUCTURE

DBE modes have been used before to miniaturize dielectric resonator antennas by lowering their resonance frequencies [6]. They have also been demonstrated to enhance the directivity of the horn antenna due to their strong resonance [37]. However, they have never been used before in high-power microwave sources, e.g., traveling wave tubes or BWOs. These sources typically require "mode purity" and an intense axial field at the center. Previously, DBE crystals [17] or rf structures [22] supported the strong resonant field. Yet, they lacked mode purity and supported hybrid modes, inapt for such applications. Since we have demonstrated that TM$_{01}$-DBE modes with mode purity can be achieved using coupled TL-based butterfly geometry, there is a strong potential for DBE mode-based tube applications. That is, the DBE mode can be useful for the electron-beam–rf-wave interaction for vacuum tubes. However, since DBE modes are associated with a narrow bandwidth, BWOs or klystrons are more appropriate applications for this. In this paper, we focus on BWO only. BWOs are active devices designed to oscillate in single frequency depending on the electron beam energy passing through it. The space-charge field of the beam couples to the backwardly propagating wave, creating a feedback path for rf energy and oscillation is established. The oscillation frequency depends on the matching of the velocity of the beam and the phase velocity of the backward wave. Typically, it is the intersecting point of the beam line

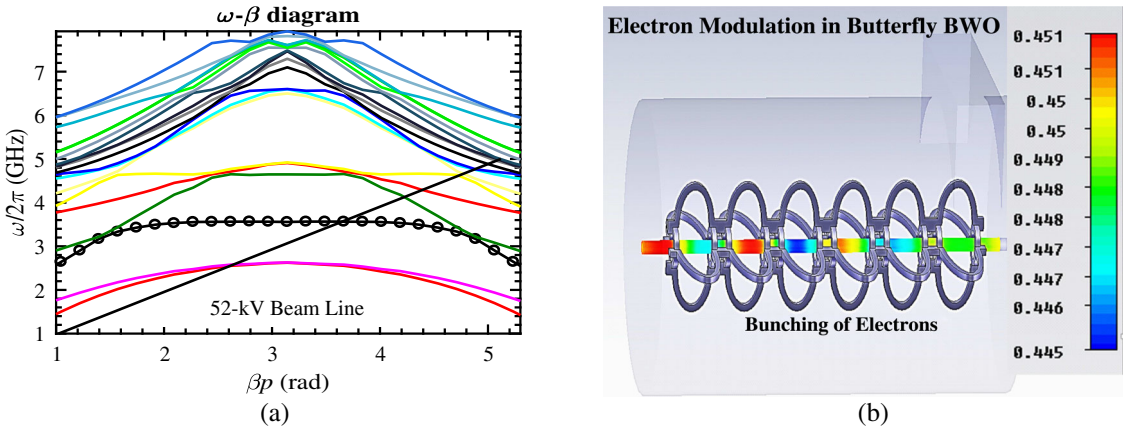

FIG. 7. (a) ω-β diagram of the first 20 modes of the butterfly slow-wave structure using HFSS [36]. A 52-kV, 4-A beam line is drawn to show the resonant point (intersecting point of the straight line and DBE mode) where beam-wave interaction takes place in a simple butterfly BWO design. (b) Demonstration of beam-wave interaction in a BWO loaded with butterfly slow-wave structure simulated using the CST PIC code [38]. The presence of bunching due to velocity modulation verifies the electron modulation process, essential for wave-particle coupling and power transfer. The color ramp shows the beam velocity v_e normalized to the speed of light c.

and ω-β diagram of the slow-wave structure. As seen in Fig. 7(a), ω-β diagrams of the first 20 modes of the butterfly slow-wave structure is given along with the 52-kV beam line. The beam will interact with all modes that have the E_z field at the center. To illustrate the BWO interaction with the DBE mode, a BWO design is simulated using the computer simulation software (CST) particle-in-cell (PIC) [38] code. The BWO draws 4-A current from a circular cathode biased at 52 kV. The tube is 16 cm long and generates 68 kW power at 3.34 GHz with 33% electronic efficiency. The butterfly slow-wave structure is placed at the center of the waveguide as shown in Fig. 7(b). The bunching of electrons verifies the beam-wave interaction [Fig. 7(b)]. Typically, the homogenous section BWOs are associated with nominal electronic efficiency of 15%–20% [39,40]. Hence, a 13%–18% efficiency improvement is observed by introducing the DBE mode in the BWO using the butterfly geometry.

V. CONCLUSION

We implement a class of TLs that can generate DbBE and DBE modes. It is demonstrated that a dual pair of nonidentical TLs can generate higher-order dispersion curves, especially DBE modes. Fourth-order dispersion equations are derived using the coupled-mode analysis for the nonidentical pair of coupled TLs. Further, it is shown that the order of the dispersion curves is dependent on the choice of coupling parameters, K_{c1}, K_{c2}, and K_{c3} and dispersion can be controlled by them. An alternate approach of DBE-mode realization inside circular waveguides is demonstrated via butterfly geometry, a design based on four coupled TLs. This geometry provides an approximately 300× stronger E_z field on the axis compared to elliptic irises. The presence of the DBE mode verifies the coupled TLs as an effective alternative of bulk photonic crystals. The same concept can be extended further to design couplers, filters, printed circuits, and to engineer a new class of vacuum tubes and BWOs. An example of BWO design is presented to verify the beam-wave interaction with the DBE TM_{01}-like mode. The BWO demonstrates efficiency improvement by 13%–18% compared to nominal BWOs. This theory and example are expected to serve as tools to engineer dispersion curves for more practical applications.

ACKNOWLEDGMENTS

This research is supported by AFOSR MURI Grant No. FA9550-12-1-0489 administered through the University of New Mexico.

[1] E. Rajo-Iglesias, O. Quevedo-Teruel, and L. Inclan-Sanchez, Mutual coupling reduction in patch antenna arrays by using a planar EBG structure and a multilayer dielectric substrate, IEEE Trans. Antennas Propag. **56**, 1648 (2008).

[2] N. Apaydin, K. Sertel, and J. L. Volakis, Nonreciprocal and magnetically scanned leaky-wave antenna using coupled CRLH lines, IEEE Trans. Antennas Propagat. **62**, 2954 (2014).

[3] F. Yang and Y. Rahmat-Samii, Microstrip antennas integrated with electromagnetic band-gap (EBG) structures: a low mutual coupling design for array applications, IEEE Trans. Antennas Propag. **51**, 2936 (2003).

[4] D. Sievenpiper, L. Zhang, R. F. J. Broas, N. G. Alexopolous, and E. Yablonovitch, High-impedance electromagnetic surfaces with a forbidden frequency band, IEEE Trans. Antennas Propag. **47**, 2059 (1999).

[5] B. Munk, *Frequency Selective Surfaces: Theory and Design* (Wiley, New York, 2000).

[6] G. Mumcu, K. Sertel, and J. L. Volakis, Miniature antenna using printed coupled lines emulating degenerate band edge crystals, IEEE Trans. Antennas Propag. **57**, 1618 (2009).

[7] C. Locker, K. Sertel, and J. L. Volakis, Emulation of propagation in layered anisotropic media with equivalent coupled microstrip lines, IEEE Microwave Wireless Compon. Lett. **16**, 642 (2006).

[8] M. B. Stephanson, K. Sertel, and J. L. Volakis, Frozen modes in coupled microstrip lines printed on ferromagnetic substrates, IEEE Microwave Wireless Compon. Lett. **18**, 305 (2008).

[9] R. A. Shelby, D. R. Smith, and S. Schultz, Experimental verification of a negative index of refraction, Science **292**, 77 (2001).

[10] C. A. Balanis, *Antenna Theory: Analysis and Design* (Wiley, New York, 2016).

[11] D. C. Chang and C. N. Hu, Smart antennas for advanced communication systems, Proc. IEEE **100**, 2233 (2012).

[12] E. Yablonovitch, Inhibited Spontaneous Emission in Solid-State Physics and Electronics, Phys. Rev. Lett. **58**, 2059 (1987).

[13] A. Figotin and I. Vitebsky, Gigantic transmission band-edge resonance in periodic stacks of anisotropic layers, Phys. Rev. E **72**, 036619 (2005).

[14] A. Figotin and I. Vitebsky, Slow-wave resonance in periodic stacks of anisotropic layers, Phys. Rev. A **76**, 053839 (2007).

[15] M. A. K. Othman, F. Yazdi, A. Figotin, and F. Capolino, Giant gain enhancement in photonic crystals with a degenerate band edge, Phys. Rev. B **93**, 024301 (2016).

[16] G. Mumcu, K. Sertel, J. L. Volakis, I. Vitebskiy, and A. Figotin, RF propagation in finite thickness unidirectional magnetic photonic crystals, IEEE Trans. Antennas Propag. **53**, 4026 (2005).

[17] S. Yarga, K. Sertel, and J. L. Volakis, Degenerate band edge crystals for directive antennas, IEEE Trans. Antennas Propag. **56**, 119 (2008).

[18] N. Apaydin, L. Zhang, and J. L. Volakis, Experimental validation of frozen modes guided on printed coupled transmission lines, IEEE Trans. Microwave Theory Tech. **60**, 1513 (2012).

[19] A. Figotin and I. Vitebsky, Nonreciprocal magnetic photonic crystals, Phys. Rev. E **63** (2001).

[20] A. Figotin and I. Vitebsky, Electromagnetic unidirectionality in magnetic photonic crystals, Phys. Rev. B **67**, 165210 (2003).

[21] J. L. Volakis and K. Sertel, Narrowband and Wideband Metamaterial Antennas Based on Degenerate Band Edge and Magnetic Photonic Crystals, in Proc. IEEE **99**, 1732 (2011).

[22] M. A. K. Othman and F. Capolino, Demonstration of a degenerate band edge in periodically-loaded circular waveguides, IEEE Microwave Wireless Compon. Lett. **25**, 700 (2015).

[23] M. A. K. Othman, M. Veysi, A. Figotin, and F. Capolino, Giant amplification in degenerate band edge slow-wave structures interacting with an electron beam, Phys. Plasmas **23**, 033112 (2016).

[24] S. Yarga, K. Sertel, and J. L. Volakis, Multilayer dielectric resonator antenna operating at degenerate band edge modes, IEEE Antennas Wireless Propag. Lett. **8**, 287 (2009).

[25] M. G. Wood, J. R. Burr, and R. M. Reano, Degenerate band edge resonances in periodic silicon ridge waveguides, Opt. Lett. **40**, 2493 (2015).

[26] V. A. Tamma, A. Figotin, and F. Capolino, Concept for pulse compression device using structured spatial energy distribution, IEEE Trans. Microwave Theory Tech. **64**, 742 (2016).

[27] S. Sensiper, Electromagnetic wave propagation on helical structures (a review and survey of recent progress), Proc. IRE **43**, 149 (1955).

[28] D. Lopes and C. Motta, Characterization of ring-bar and contrawound helix circuits for high-power traveling-wave tubes, IEEE Trans. Electron Devices **55**, 2498 (2008).

[29] M. Zuboraj and J. L. Volakis, Curved ring-bar slow-wave structure for wideband MW-power traveling wave tubes, IEEE Trans. Plasma Sci. **44**, 903 (2016).

[30] S. Liu, Calculation of the parameters for ring-loop traveling wave tube in MMW, Int. J. Infrared Millim. Waves **21**, 1097 (2000).

[31] D. Watkins, *Topics in Electromagnetic Theory* (Wiley, New York, 1958).

[32] D. Marcuse, *Theory of Dielectric Optical Waveguides*, 2nd ed. (Academic Press, New York, 1991).

[33] J. Pierce, Coupling of Modes of Propagation , J. Appl. Phys. **25**, 179 (1954).

[34] See Supplemental Material at http://link.aps.org/supplemental/10.1103/PhysRevApplied.7.064030 for detailed derivation of the coupled mode propagation constants in continuously coupled systems.

[35] *CST Microwave Studio, User Manual* (Computer Simulation Technology, GmbH, Darmstadt, Germany, 2016).

[36] *Ansoft HFSS 15, User Manual* (Ansys Corp., Canonsburg, PA, 2015).

[37] S. Yarga, K. Sertel, and J. L. Volakis, Degenerate Band Edge Crystals and Periodic Assemblies for High Gain Antennas, in *Proceedings of the 2006 IEEE Antennas and Propagation Society International Symposium* (IEEE, Albuquerque, NM, 2006), pp. 7–10.

[38] *CST Particle Studio, User Manual* (Computer Simulation Technology, GmbH, Darmstadt, Germany, 2015).

[39] B. Levush, T. M. Antonsen, A. N. Vlasov, G. S. Nusinovich, S. M. Miller, Y. Carmel, V. L. Granatstein, W. W. Destler, A. Bromborsky, C. Schlesiger, D. K. Abe, and L. Ludeking, High-efficiency relativistic backward wave oscillator: theory and design, IEEE Trans. Plasma Sci. **24**, 843 (1996).

[40] Z. Wang, Y. Gong, Y. Wei, Z. Duan, Y. Zhang, L. Yue, H. Gong, H. Yin, Z. Lu, J. Xu, and J. Feng, High-power millimeter-wave BWO driven by sheet electron beam, IEEE Trans. Electron Devices **60**, 471 (2013).